Investigation into crystal structure using X-ray spectroscopy to determine lattice constants and the Rydberg constant

Kacper Slodek
School of Physics, University of Bristol
(Dated: December 2023)

The values for lattice constants for NaCl and Si crystals were found using an X-ray diffraction apparatus to be $a = (5.63 \pm 0.01)$Å compared to a literature value of $a = 5.60$Å and $a = (5.43 \pm 0.02)$ compared to $a = 5.431$Å respectively. The computed Rydberg constant, $R_\infty = (11 \pm 2) \times 10^6\ \mathrm{m}^{-1}$, demonstrated a minimal 0.2% difference from the literature value. The theoretical model of the structure factor was verified through relfection from crystal planes in both solid NaCl crystal and powder samples.

I. Introduction

X-ray photons are typically classified into two categories: those with energies of $0.12keV < E < 12keV$, as 'soft' X-rays and those with energies of $12keV < E < 120keV$. The main difference is that 'soft' X-ray measurements usually require a vacuum setup whereas 'hard' X-rays can be used at ambient conditions [1]. The uses of X-ray radiation range from spectroscopy of cooling clusters of galaxies to investigate their temperature [2], to medical uses like the X-ray computer tomography which uses radiation to reconstruct images used in diagnoses [3]. One of the most vital uses of this kind of radiation is crystal spectroscopy, also known as crystallography, which utilises the interaction between the X-ray photons and matter, like the crystal lattices, to examine their physical structure [4], like examining the electronic structure investigation of $Cu_2CdGeSe_4$ carried out by V.A. Ocheretova [5]. X-rays are used in crystallography, as their wavelengths are similar to the spacing between atoms in crystal lattices, this allows the scattering of the X-ray photons to probe the arrangement and relative size of atoms within the crystal. It is also widely utilised to probe properties like elementary excitations with the use of resonant inelastic X-ray scattering [6].

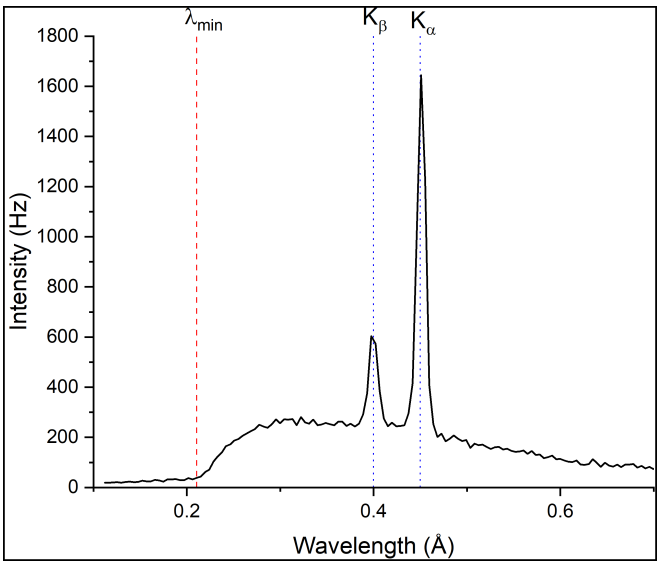

FIG. 1: X-ray spectrum of LiCl crystal sample with (200) planes parallel to the surface of crystal. The two characteristic lines seen are the first order K_α and K_β lines of Molybdenum, while the λ_{min} is the characteristic wavelength at which the bremsstrahlung radiation starts to emit particles.

X-ray spectra produced during crystallography usually measure the intensity of radiation detected against the wavelength of that radiation (see Figure 1 for example spectrum), from this, various information can be deduced like the elemental composition of a sample, its chemical state and structure, as well as electronic configuration and energy states of atoms within the sample.

II. Theory

A. Crystal Structure and Miller indices

Every crystal is made of a lattice, which is built of repeating unit cells [7]. This periodic arrangement causes the crystal lattices to exhibit certain properties when interacting with X-ray radiation. It is useful to think of each unit cell's interaction individually to study the combined interaction of the whole lattice. Assuming some arbitrary length for the unit cell, like 1, one can describe the fractional position coordinates of atoms in the unit cell to illustrate the structure of the unit cell [8].
Generally, the lattice constants are lengths and angles which represent the geometry of the crystal [9]; to completely specify the geometry, three lengths (a, b, c) and three angles (α, β, γ) are needed, however in the special case where the crystal is cubic, $\alpha = \beta = \gamma = \pi/2$, and $a = b = c$, so only a single lattice parameter, a is needed to describe the dimensions of the crystal. This lattice constant describes how often (spatially) the unit cell structure repeats. Such crystals were studied in this investigation, namely NaCl, LiCl and Si.
Miller indices are used to signify points and planes in crystal lattices that help describe their properties [10]:

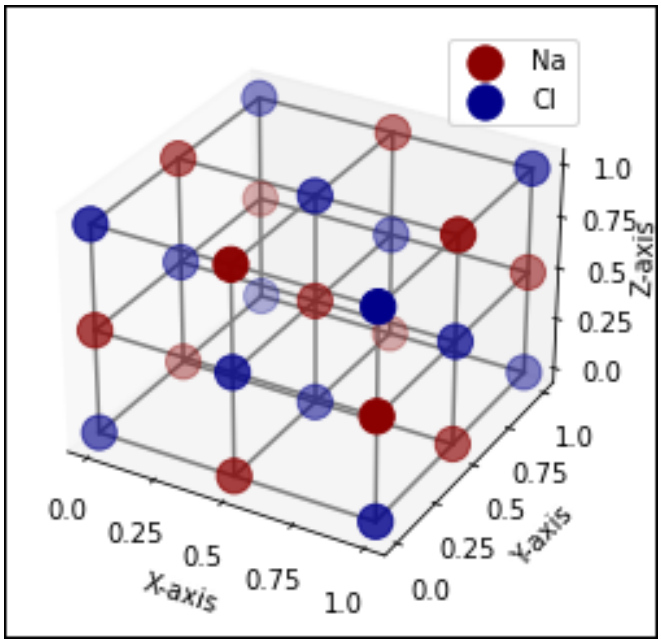

FIG. 2: A unit cell of NaCl crystal with an arbitrary lattice constant $a = 1$; the central Na^+ atom has fractional coordinates $(\frac{1}{2}, \frac{1}{2}, \frac{1}{2})$. It is an example of an FCC (face-centred cubic) crystal.

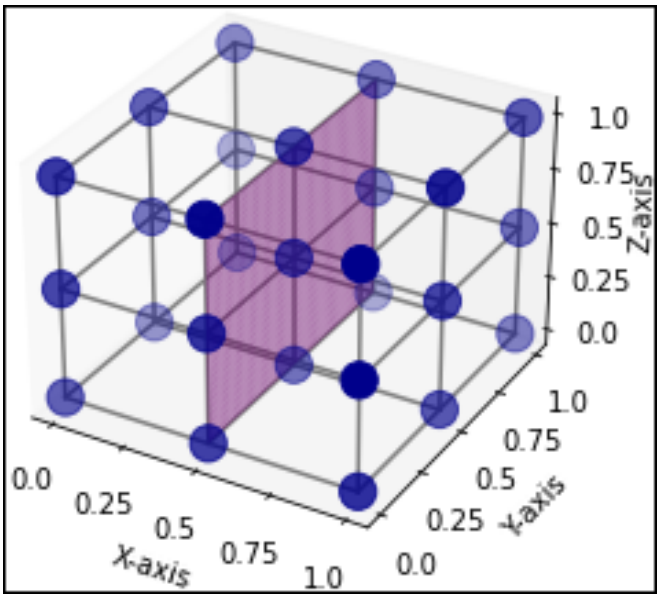

FIG. 3: A visual representation of the (200) plane in an arbitrary simple cubic crystal lattice. The plane crosses the x-axis at $x = 1/2$. Since it does not cross the y or z axes, conventionally it is said that the plane crosses these axes at $y = z = \infty$ so that the reciprocal, and therefore the Miller plane is $(1/(1/2)\ 1/\infty\ 1/\infty) = (200)$.

(h, k, l) represents a point, whereas (hkl) represents a plane, these are derived from the points where the plane crosses the axes, i.e. the plane crossing the x-axis at $x = a$, y-axis at $y = b$ and the z-axis at $z = c$, the coordinates of this plane could be described as (a, b, c). Then taking the reciprocals of these coordinates, one can obtain the Miller plane:

$$(hkl) = (\frac{1}{a}\frac{1}{b}\frac{1}{c}). \tag{1}$$

This utilises the reciprocal space in the description of planes to simplify the diffraction pattern from the crystal planes, which can be shown as being equivalent to the Fourier transform of the 'slit pattern' (plane spacing in case of a crystal lattice), and therefore it is innately represented by the reciprocal space [11]. The spacing between adjacent (hkl) planes in a cubic lattice can be shown to be [12]:

$$d_{hkl} = a/\sqrt{h^2 + k^2 + l^2}, \tag{2}$$

where a is the lattice constant of the lattice and $h, k, l \in \mathbb{N}$.

B. X-ray production and interaction

In an X-ray tube, there are two main ways that X-rays are produced: Firstly, Bremsstrahlung, which arises from electrons losing kinetic energy due to deflection by another charged particle [13] (typically the nucleus of an atom). This energy is transferred to a photon via the law of conservation of energy such that $KE_{e^-} = hf$, where f is the frequency of the produced photon and h is the Planck's constant.

Secondly, the characteristic X-ray production is a process if an incident electron has more energy than the binding energy of an orbiting electron in an atom. This orbiting electron is then ejected, which creates a vacant space in an electron shell, which an outer electron fills, releasing energy as a photon satisfying $E_n - Em = hf$ [14]. Since this frequency is dependent on the energy levels, it is characteristic of each element. Specifically, there are two prominent transitions within this effect: when an electron from the second shell drops to the first shell, this emission line is known as K_α. Similarly, when an electron transitions from the third to the first shell, the emission line is known as K_β (both can be seen on Figure 1).

When X-rays hit crystal lattice, they can diffract, since their wavelength is similar to the inter-atomic spacing within crystals. The local maximum intensity of the pattern occurs when the Bragg condition is fulfilled [15]:

$$n\lambda = d_{hkl} \sin\theta, \tag{3}$$

where n is the diffraction order, λ is the wavelength and θ is the angle of incidence, measured from the surface of the crystal sample.

Moreover, when a photon with enough energy interacts with an orbiting electron in an atom, it can be absorbed to promote the electron to a higher shell. This can create absorption spectra, revealing a phenomenon similar to the aforementioned characteristic wavelengths [16]. This wavelength, λ of the characteristic absorption is related to the number of protons, Z in the nucleus of an atom such that:

$$\lambda^{-1/2} = R_{\infty}^{-1/2}(Z - \sigma), \tag{4}$$

where R_{∞} is the Rydberg constant for heavy atoms and σ is the screening coefficient arising due to the electric field in the atom.

Finally, the structure factor can be used to determine the amplitude (and therefore intensity) and phase of the X-ray beams reflected from the crystal. For a given plane (hkl), the structure factor is a sum over all atoms in a unit cell such that [17]:

$$F_{hkl} = \sum_{p=1}^{N} f_p e^{-2\pi i(hx_p + ky_p + lz_p)}, \tag{5}$$

where f_p is the scattering factor attributed to the pth atom, and (x_p, y_p, z_p) are the fractional coordinates of the atom within the unit cell. This formula can be used to predict whether or not a certain plane will exhibit a reflection, and if so, how intense the reflection will be, as generally, if the intensity of the reflection is I, then $I \propto |F_{khl}|^2$.

III. Method

A standard X-ray tube was used to provide the beam for the diffraction, using a molybdenum target as the anode (see Figure 4). The filament cathode is heated by passing enough current through it, that thermionic emission of electrons is possible. Those electrons are then accelerated across to the molybdenum anode, where either Bremsstrahlung or characteristic emission (described in Section 2B) takes place. The X-ray photon beam then was narrowed using the collimator - a device comprised of very narrow plates that caused the produced rays to become parallel, so that they could hit the sample at a desired angle.

The collimated X-rays next entered the target crystal and were diffracted towards the detector, which recorded the received count rate of radiation. The tube voltage was set to the maximum value of $V = 35kV$ as was the tube current at $I = 1mA$. This allowed for the maximum possible intensity of produced X-rays to probe the crystal samples. Both the sample stage and the detector could rotate through a range of angles, with the used (and the smallest) angle step $\Delta\beta = 0.1^{\circ}$, to achieve the best possible resolution for peak analysis. The time step that the apparatus spent on each angle could be varied as well, and was changed depending on the circumstances (discussed later) to enable the distinction of values like peaks from the baseline.

The apparatus had multiple spectrum settings, however, the most relevant one was the 'coupled' one, which meant that the detector angle was always twice the sample goniometer angle. This allowed for a good range of angles' reflections to be investigated.

Each sample was inserted into the holding cradle on the sample stage and firmly screwed in to prevent any unwanted movement of the sample which could disturb the shape of the spectrum and therefore could ruin the results of the experiments. Before the tube was turned on, the apparatus was checked for any leaking radiation using a portable Geiger counter to ensure safety during the experiment.

A. Lattice Constant

To obtain the lattice constant, a of each sample, a 'sweep' across a range of angles $2.5^{\circ} < \beta < 30.0^{\circ}$, with a time step of $\Delta t = 3s$. An example spectrum produced using this method can been seen in Figure 1 (with angle translated to wavelength using Equation 3). The spectra had visible peaks resulting from the molybdenum anode with manufacturer-provided characteristic wavelengths of $K_{\beta} = 63.1pm$ and $K_{\alpha} = 71.1pm$. The peaks were selected by using the first and second derivatives of the spectrum to investigate where the spectrum goes through a maximum. The pairs of these peaks were attributed to consecutive orders of diffraction, $n = 1, 2, 3$; this meant that a plot of $n\lambda$ obtained from the peaks, against the sine of the angle θ would in theory produce a straight line with gradient $m = d_{hkl}$. The crystal samples used in the spectroscopy had the information about which planes were parallel to the surface of the crystal, therefore (hkl) was known. From this gradient, and Equation 2, the lattice constant could be obtained from

$$a = d_{hkl}\sqrt{h^2 + k^2 + l^2}. \tag{6}$$

This could then be used to calculate the maximum theoretical density of the crystal using the equation

$$\rho = \frac{\sum_{j=1}^{N} m_j}{a^3}, \tag{7}$$

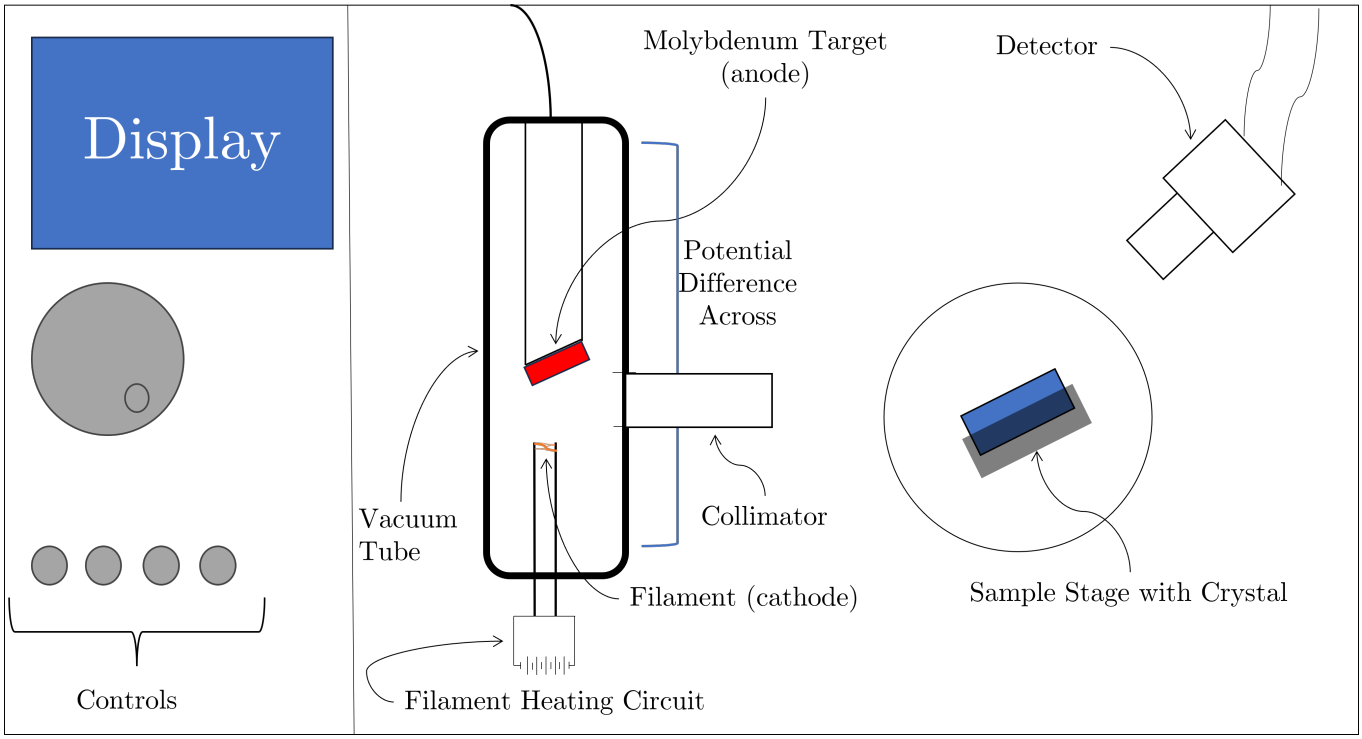

FIG. 4: X-ray spectroscopy apparatus with a molybdenum anode. The potential difference was set to $V = 35kV$ and the current $I = 1mA$. The apparatus was connected to a computer interface which plotted the spectra as they were taken and allowed the export of values into other programs for further analysis.

where m_j is the mass of an atom within a unit cell of an atom, summed over N atoms in a unit cell. Importantly, within a unit cell, many unit cells share one atom, so this had to be taken into account in the calculation.

B. Rydberg Constant

In order to obtain the Rydberg constant, a range of metal caps were applied on the collimator and new spectra of NaCl were taken. The intensity array of each metal cap spectrum was divided by a 'clean' spectrum of NaCl crystal to create transmission spectra $T_Z = R_Z/R_0$, where Z is the atomic number of the metal inside the cap. The minima of these transition spectra were obtained using a method similar to the one used for peaks in the previous section. Theoretically, the minima would occur at the characteristic absorption wavelength of each metal.

Plotting the reciprocal of the square root of these characteristic wavelengths against the atomic number of each element cap would produce a linear plot with gradient $m = R_\infty^{-1/2}$. Therefore, the Rydberg constant could be obtained by rearranging such that $R_\infty = 1/m^2$.

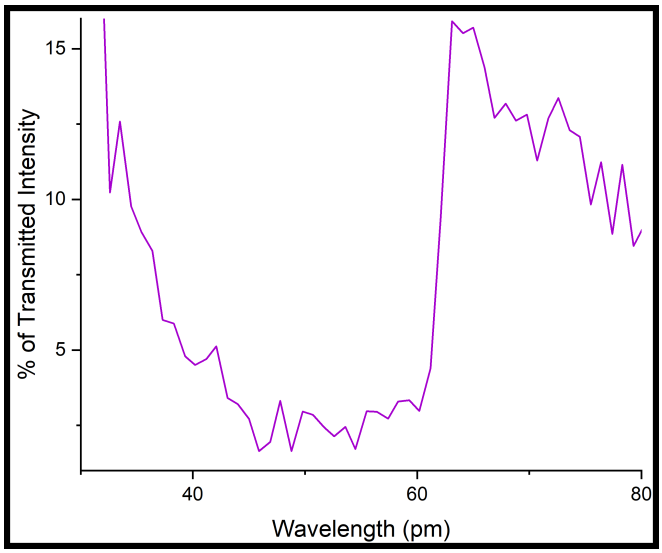

FIG. 5: Transmission spectrum of Niobium cap ($Z = 41$). The minimum occurs at the characteristic absorption wavelength of the metal cap (around $\lambda = 60pm$).

IV. Results

A. Lattice constant

The plots of $n\lambda/2$ against $sin(\theta)$ have shown a clear linear relationship as predicted by the theoretical model of Bragg peaks introduced in Equation 3.

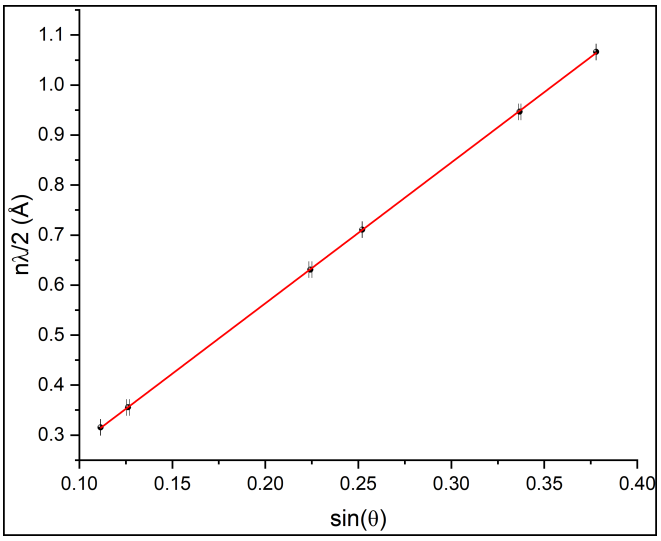

FIG. 6: Linear fit of the plot of $n\lambda/2$ against $sin(\theta)$ for NaCl crystal with (200) planes parallel to the surface of the crystal. The lattice spacing $d_{200} = (2.815 \pm 0.007)$Å. Therefore the lattice constant was $a = (5.63 \pm 0.01)$Å.

The NaCl lattice constant was found to be $a = (5.63 \pm 0.01)$Å, compared to a literature value of $a = 5.60$Å [18], with just a 0.5% difference. This was found using Equation 6 from the gradient (of the plot from Figure 6) as the NaCl crystal had the (200) planes parallel to the surface, $a = d_{200}\sqrt{2^2} = 2d_{200}$. To calculate the theoretical maximum density, the number of protons and neutrons that are present in the unit cell was used, which resulted in $\rho_{max} = (2.18 \pm 0.01)gcm^{-3}$, compared to a literature value of $\rho = 2.17gcm^{-3}$ [19], showing a 0.5% difference.

The silicon crystal sample had (111) planes parallel to the surface, so the gradient of the graph in Figure 7 yielded the gradient d_{111}, so the lattice constant was $a = \sqrt{3}d_{111}$. This lattice constant was found to be $a = (5.43 \pm 0.02)$Å, compared to the literature value of $a = 5.4310199$Å [20], this shows a staggering 0.02% difference. Using a similar method to the density of NaCl, the theoretical maximum density of silicon crystal was found to be $\rho_{max} = (2.34 \pm 0.03)gcm^{-3}$, compared to the literature value of $\rho = 2.32902gcm^{-3}$ [21], exhibiting a 0.5% difference. The lithium chloride crystal, having a structure identical to NaCl, albeit with one of the constituents being a smaller atom (Lithium vs. Sodium), amounted to a smaller lattice constant of $a = (5.0 \pm 0.1)$Å, and density of $\rho_{max} = (2.2 \pm 0.1)gcm^{-3}$, compared to the literature values of $a = (5.038 \pm 0.022)$Å [22] (0.8% difference) and $\rho = 2.07gcm^{-3}$ [23] (6.3% difference) respectively.

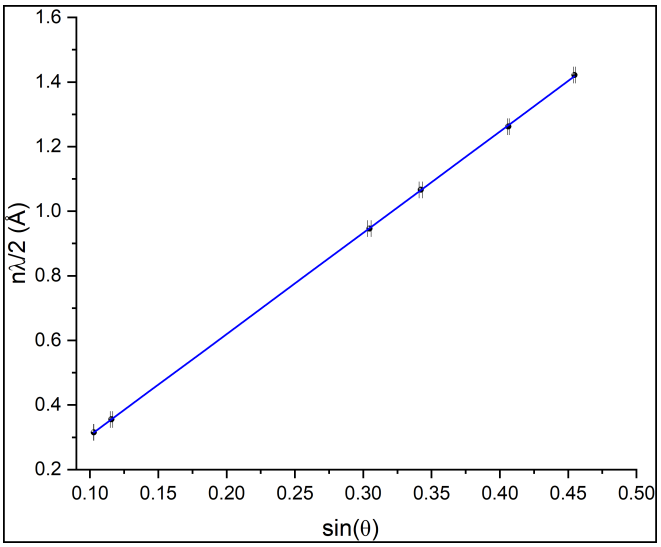

FIG. 7: Linear fit of the plot of $n\lambda/2$ against $sin(\theta)$ for NaCl crystal with (200) planes parallel to the surface of the crystal. The lattice spacing $d_{200} = (2.815 \pm 0.007)$Å. Therefore the lattice constant was $a = (5.63 \pm 0.01)$Å.

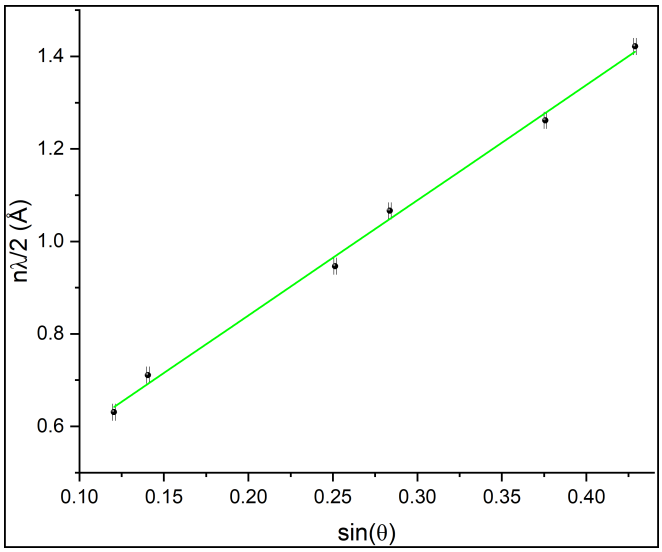

FIG. 8: Linear fit of the plot of $n\lambda/2$ against $sin(\theta)$ for LiCl crystal with (200) planes parallel to the surface of the crystal. The lattice spacing $d_{200} = (2.49 \pm 0.007)$Å. Therefore the lattice constant was $a = (5.0 \pm 0.1)$Å.

B. Rydberg Constant

Five different collimator caps made from different metals were used to measure the Rydberg constant. The linear relationship observed in the plot of the reciprocal of the square root of the characteristic absorption wavelength against the atomic number (Figure 9) confirms the model postulated in Equation 4, with the Rydberg constant obtained $R_\infty = (12 \pm 2) \times 10^6 m^{-1}$

including the outlier at $Z = 41$ and $R_\infty = (11 \pm 2) \times 10^6 m^-1$ without it. These values were compared to a literature value of $R_\infty = 10.97373157 \times 10^6 m^-1$ [24], resulting in a 9.4% difference using the outlier value and a 0.2% difference ignoring the outlier.

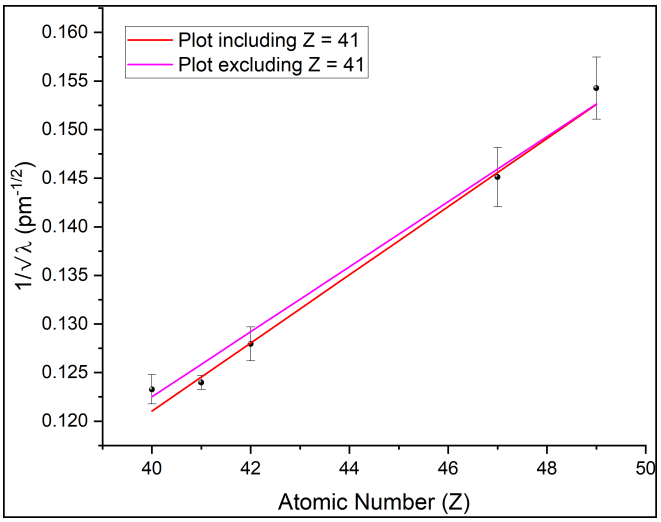

FIG. 9: Linear fit of the inverse square wavelength of absorption peaks of different metals against their atomic number. The gradient of the line excluding $Z = 41$ was $m = (3.83 \pm 0.04) \times 10^3 m^{-1/2}$ corresponding to Rydberg constant of $R_\infty = (12 \pm 2) \times 10^6 m^-1$, whereas the line including all Z had gradient $m = (4.2 \pm 0.4) \times 10^3 m^{-1/2}$, and $R_\infty = (11 \pm 2) \times 10^6 m^{-1}$.

C. Powder NaCl

A spectrum of powder NaCl sample was also investigated to examine the reflections from planes different than (200). This has resulted in a spectrum with significantly more peaks than the solid crystal sample. All theoretically possible planes from which there would be reflections present and their approximate intensity were calculated using a dedicated program written to utilise Equation 5 to sum over the atoms within a crystal lattice. Since NaCl is a cubic lattice, there was a lot of degeneracy in the spectrum, where planes like (200), (020), (002) were practically identical since the sample contained randomly aligned crystals; this meant that the planes are the same, just rotated 90° about one of the three axes.

V. Discussion

A. Error Calculation

The errors in values were calculated using the partial derivative error propagation method. For instance, in the error of density of crystal, the only variable was the lattice constant a. Therefore the error on the density

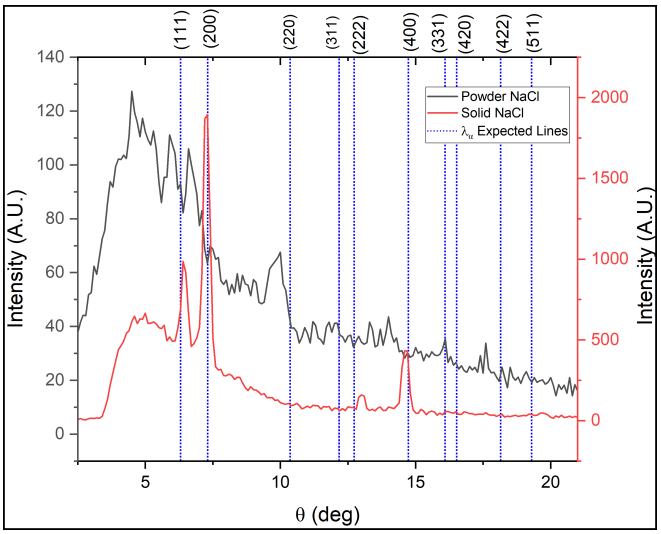

FIG. 10: Spectra of solid and powder NaCl for a range of angles. It can be seen that the solid sample with (200) planes parallel to the surface of the crystal exhibits the largest intensity diffraction from the (200) and (400) planes with smaller, but still present reflections from (111) and (222) planes. Theoretical reflection lines retrieved from [25].

$(\Delta\rho)$ was calculated using the following formula:

$$(\Delta\rho)^2 = (\frac{\partial\rho}{\partial a}\Delta a)^2 = \left(\frac{-3\sum_{j=1}^{N} m_j}{a^4}\right)^2. \qquad (8)$$

Similarly, the error on lattice constant from plane spacing was $\Delta a = \Delta d_{hkl}\sqrt{h^2+k^2+l^2}$. The error on each measurement of peaks in the diffraction or absorption spectra was taken as ± half the range of values taken to approximate the peak using the derivative method. These errors carried on to the error of the gradients of the lines produced in Figures 6-9. To increase the precision and consistency of all the results, another method of choosing peaks could have been used instead. Namely, fitting the peaks to a Lorentzian function [26] would result in an estimate of the parameters of a Lorentz peak to establish a more consistent error on the location of a peak within a spectrum, thus increasing the precision of all the results that followed (lattice constant, density and Rydberg constant).

B. Method Improvements

The accuracy of the results might have been influenced by systematic errors in the method. One such error in the spectra of NaCl and LiCl could have come from the fact that both these compounds are hygroscopic [27][28]. The partial dissolution of these crystals due to moisture absorption from the air could have led to unwanted effects on the experiment's results.

Firstly, the shape of the crystal lattice could have been partly altered, resulting in a deviation from the expected diffraction patterns. Secondly, the presence of water on or around the crystals could have had the effect of refracting the X-rays, potentially misrepresenting the count rate at certain angles. This could have been remedied using methods like heat treating the samples, desiccation using silica gel, or vacuum drying [29]. This would ensure there is a minimal amount of moisture in the samples to contribute to misrepresentation of the results.

This approach could be generalised, as the lack of control over the smoothness and purity of the provided samples could have led to deviation from the theoretical model. Small imperfections or perforations in the crystals could introduce unwanted scattering effects. These imperfections could have potentially interfered with the X-rays at various phases, leading to the generation of noise or diminishing the intensity of the peaks of interest in the spectra. To address this issue, one could ensure that from the initial cutting of the crystal sample, to their insertion into the apparatus, the sample was handled with utmost care in a sterile environment. This would ensure no oil from the skin would be transferred onto the surface of the sample. Such careful handling would minimise the risk of damage and contamination, therefore enhancing the quality of the diffraction data obtained and the results.

Another improvement of precision of the experiment would be if the resolution of the spectroscopy apparatus was better: the smallest angle step available to be selected was $\Delta\beta = 0.1°$. This made it difficult to decide where the peaks or k-edges were, as evident in Figure 5. This impacted every part of the experiment, as if the resolution was any better, the peaks and k-edges would be resolved better, and their location would be more certain, translating to a more accurate and precise results. This could be achieved with a more sophisticated, circuit-driven goniometer with a better resolution. Current technology, like the one used by Y. Imai allows for angular resolutions as small as $\Delta\beta = 4.6 \times 10^{-3}°$ in X-ray spectroscopy [30].

Another improvement to the method could be to use a more efficient source of X-rays, as the apparatus used was only about 1% efficient with converting energy to X-ray photons (according to the manufacturer). One replacement of the tube could be a synchrotron radiation source which accelerates electrons, which emit X-ray radiation when they change direction [31]. This would ensure improved intensity, which would make later diffraction orders more pronounced, enabling more data points for the lattice constant calculation, and leading to an increase in accuracy and precision. Moreover, beams produced by the synchrotron can be focused with incredible precision to ensure the best possible accuracy of incident angle.

To improve the precision of the value of the Rydberg constant, a wider range of collimator caps used as filters could have been used. This would have resulted in more data points for the linear fit seen in Figure 9. Replacing the niobium cap with a different one could also improve the accuracy and precision of the result since multiple spectra were taken, and the k-edge resulting from the transmission of $Z = 41$ cap was always an outlier.

The powder spectrum seen in Figure 10 contains a significant amount of noise, especially in the low-angle range. This was because the sample was not secured in place therefore the powder would slide down if the sample stage goniometer was turned through an angle. Instead, the detector only was turned, while the stage was stationary. This resulted in the non-diffracted X-rays from the tube entering the detector in the small angle territory, and influencing the spectrum. Additionally, powdered NaCl was more susceptible to the hygroscopic effects mentioned before. This can explain the systematic displacement of peaks from their theoretical position (for example the (220) peak). An obvious solution to this is securing the sample from the top with an X-ray transparent material, like beryllium [32].

VI. Conclusion

Despite possible sources of error, the theoretical model of Bragg peaks and Moseley's law were confirmed. The values of lattice constants were found for a range of solid crystal samples.

Material	Calculated a	Literature a	% Difference
NaCl	(5.63 ± 0.01)Å	5.60Å	0.5%
Si	(5.43 ± 0.02)Å	5.431Å	0.02%
LiCl	(5.0 ± 0.1)Å	5.038Å	0.8%

TABLE I: Comparison of calculated and theoretical values of the lattice constant for a range of materials.

Similarly, the theoretical maximum density of those materials was calculated and compared against literature values

Material	Calculated ρ_{max}	Literature ρ	% Difference
NaCl	$(2.18 \pm 0.01) gcm^{-3}$	$2.17 gcm^{-3}$	0.5%
Si	$(2.34 \pm 0.03) gcm^{-3}$	$2.3290 gcm^{-3}$	0.5%
LiCl	$(2.2 \pm 0.1) gcm^{-3}$	$2.07 gcm^{-3}$	6.3%

TABLE II: Comparison of calculated and theoretical values of material density for a range of materials.

Moreover, the value of the Rydberg constant was calculated to be $R_\infty = (11 \pm 2) \times 10^6 m^-1$ compared to the literature value of $R_\infty = 10.97373157 \times 10^6 m^-1$, giving a 0.2% difference. The theoretical model of structure factor has been confirmed with the peak intensity from different crystal planes being calculated and fitted to theoretical angular positions for both a solid NaCl crystal, and NaCl powder.

References

[1] Ramesh C. Gupta. *Reproductive and Developmental Toxicology*. 2011. Chap. 75, p. 984.

[2] J.R. Peterson and A.C. Fabian. "X-ray spectroscopy of cooling clusters". In: *Physics Reports* 427.1 (2006), pp. 1–39.

[3] Willi A. Kalender. "X-ray computed tomography". In: *Physics in Medicine Biology* 51.13 (2006).

[4] Simon Duckett. *Foundations of spectroscopy*. Oxford University Press, 2000.

[5] V.A. Ocheretova et al. "Electronic structure of Cu2CdGeSe4 single crystal as determined from X-ray spectroscopy data". In: *Materials Chemistry and Physics* (2015).

[6] Luuk J. P. Ament et al. "Resonant inelastic x-ray scattering studies of elementary excitations". In: *Reviews Of Modern Physics* (2011).

[7] C. Kittel. *Introduction to Solid State Physics*. 8th ed. John Wiley Sons, 2004, pp. 3–4.

[8] E. Tedesco et al. "Ab initio structure determination of a peptide b-turn from powder X-ray diffraction data". In: *Chemical Communications* (2001), pp. 1460–1461.

[9] C. Kittel. *Introduction to Solid State Physics*. 8th ed. John Wiley Sons, 2004, p. 17.

[10] R. J. D. Tilley. *Understanding Solids*. Wiley, 2005, p. 119.

[11] E. G. Steward. *Fourier Optics - An Introduction*. Dover Publications, 2011, pp. 63–64.

[12] Yoshio Waseda et al. *X-Ray Diffraction Crystallography*. Springer Berlin Heidelberg, 2011, p. 75.

[13] Werner Nakel Eberhard Haug. *The Elementary Process of Bremsstrahlun*. World Scientific, 2004, p. 15.

[14] N. A. Dyson. "Characteristic X-rays - A still developing subject". In: *Physics in Medicine Biology* (1975), pp. 2–5.

[15] C. G. Pope. "X-Ray Diffraction and the Bragg Equation". In: *Journal of Chemical Education* (1997), pp. 129–130.

[16] Bipin K. Agarwal. *X-Ray Spectroscopy: An Introduction*. Springer Berlin, 1991, pp. 53–54.

[17] U. Shmueli. *Theories and techniques of crystal structure determination*. OUP Oxford, 2007, p. 130.

[18] M.. Cohen S. Froyen. "Structural Properties of NaCl". In: *Physical Review B* (1984), pp. 3770–3771.

[19] W. Haynes. *CRC Handbook of chemistry and physics : a ready reference book of chemical and physical data*. CRC Press, 2011, p. 4.89.

[20] Y. Okada. *Properties of Crystalline Silicon*. INSPEC, 1999, p. 91.

[21] A. Smakula V. Sils. "Precision Density Determination of Large Single Crystals by Hydrostatic Weighing". In: *Physical Review Journals* (1955).

[22] K. Chruszcz-Lipska et al. "Study of the Structure and Infrared Spectra of LiF, LiCl and LiBr Using Density Functional Theory (DFT)". In: *Materials (Basel)* (2023), p. 4.

[23] D. R. Lide. *CRC Handbook of Chemistry and Physics*. 86th ed. CRC Press, 2006, p. 4.70.

[24] P. Zhao et al. "Remeasurement of the Rydberg constant". In: *Physical Review A* (1986), pp. 5139–5142.

[25] The Materials Project. "Materials Data on NaCl by Materials Project". In: (July 2020). Data retrieved from the Materials Project for NaCl (mp-22862) from database version v2023.11.1.

[26] G. K. Wertheim et al. "Determination of the Gaussian and Lorentzian content of experimental line shapes". In: *Review of Scientific Instruments* (2003), pp. 1369–1370.

[27] M. Wise et al. "Hygroscopic behavior of NaCl-bearing natural aerosol particles using environmental transmission electron microscopy". In: *Journal of Geophysical Research* (2007), pp. 3–5.

[28] A. Prakash et al. "Effects of size on water vapour absorption and regeneration in lithium chloride nanocrystals". In: *Materials Today Communications* (2023), pp. 5–7.

[29] J. M. Laux et al. "X-ray Photoelectron Spectroscopy Studies of the Effects of Water Vapor on Ultrathin Nitrate Layers on NaCl". In: *J. Phys. Chem.* (1996).

[30] Y. Imai. "High-Angular-Resolution Microbeam X-Ray Diffraction with CCD Detector". In: *AIP Conference Proceedings* (2010), pp. 30–31.

[31] M. Hart. "Synchrotron Radiation- Its Application to High-Speed, High-Resolution X-ray Diffraction Topography". In: *Journal of Applied Crystallography* (1975), pp. 436–438.

[32] Christian G. et al. *Beryllium parabolic refractive x-ray lenses*. Vol. 4783. SPIE, 2002, pp. 10–18.